AFRL-DE-PS-TR-1998-1017

AFRL-DE-PS-
TR-1998-1017

EXTENSION OF THE PERIODIC HYBRID FINITE ELEMENT METHOD FOR EXTERNAL STRATIFIED DIELECTRICS

Daniel T. McGrath, LtCol, USAF

March 1998

19980428 062

Interim Report

APPROVED FOR PUBLIC RELEASE; DISTRIBUTION IS UNLIMITED.

AIR FORCE RESEARCH LABORATORY
Directed Energy Directorate
3550 Aberdeen Ave SE
AIR FORCE MATERIEL COMMAND
KIRTLAND AIR FORCE BASE, NM 87117-5776

DTIC QUALITY INSPECTED 3

AFRL-DE-PS-TR-1998-1017

Using Government drawings, specifications, or other data included in this document for any purpose other than Government procurement does not in any way obligate the U.S. Government. The fact that the Government formulated or supplied the drawings, specifications, or other data, does not license the holder or any other person or corporation; or convey any rights or permission to manufacture, use, or sell any patented invention that may relate to them.

This report has been reviewed by the Public Affairs Office and is releasable to the National Technical Information Service (NTIS). At NTIS, it will be available to the general public, including foreign nationals.

If you change your address, wish to be removed from this mailing list, or your organization no longer employs the addressee, please notify AFRL/DEHE, 3550 Aberdeen Ave SE, Kirtland AFB, NM 87117-5776.

Do not return copies of this report unless contractual obligations or notice on a specific document requires its return.

This report has been approved for publication.

Daniel T. McGrath

DANIEL T. MCGRATH, LtCol, USAF
Project Manager

FOR THE COMMANDER

Eileen M. Walling

EILEEN M. WALLING, LtCol, USAF
Chief, High Power Microwave Division

R. Earl Good

R. EARL GOOD, SES, DAF
Director, Directed Energy Directorate

REPORT DOCUMENTATION PAGE

Form Approved
OMB No. 0704-0188

Public reporting burden for this collection of information is estimated to average 1 hour per response, including the time for reviewing instructions, searching existing data sources, gathering and maintaining the data needed, and completing and reviewing the collection of information. Send comments regarding this burden estimate or any other aspect of this collection of information, including suggestions for reducing this burden, to Washington Headquarters Services, Directorate for Information Operations and Reports, 1215 Jefferson Davis Highway, Suite 1204, Arlington, VA 22202-4302, and to the Office of Management and Budget, Paperwork Reduction Project (0704-0188), Washington, DC 20503.

1. AGENCY USE ONLY *(Leave blank)*

2. REPORT DATE
11 Mar 98

3. REPORT TYPE AND DATES COVERED
Interim, Jun 97 - Mar 98

4. TITLE AND SUBTITLE
Extension of the Periodic Hybrid Finite Element Method for External Stratified Dielectrics

5. FUNDING NUMBERS
PE: 62601F
PR: 5797
TA: AK
WU: 10

6. AUTHOR(S)
Daniel T. McGrath, LtCol, USAF

7. PERFORMING ORGANIZATION NAME(S) AND ADDRESS(ES)
Air Force Research Laboratory
Directed Energy Directorate (AFRL/DEHE)
3550 Aberdeen Ave. SE
Kirtland AFB, NM 87117-5776

8. PERFORMING ORGANIZATION REPORT NUMBER
AFRL-DE-PS-TR-1998-1017

9. SPONSORING/MONITORING AGENCY NAME(S) AND ADDRESS(ES)

10. SPONSORING/MONITORING AGENCY REPORT NUMBER

11. SUPPLEMENTARY NOTES

12a. DISTRIBUTION AVAILABILITY STATEMENT
Approved for Public Release;
Distribution Unlimited

12b. DISTRIBUTION CODE

13. ABSTRACT *(Maximum 200 words)*

The periodic hybrid finite element method was previously developed to calculate the transmission and reflection properties of general planar periodic structures, including active reflection coefficient and active element gain of phased array antennas. One of its limitations was that a unit cell of the entire material structure had to be included in the finite element region, which is inefficient when the structure includes uniform dielectric layers such as radomes and wide-angle impedance matching layers. This report presents a method for incorporating the effects of stratified exterior dielectric layers into the periodic radiation condition. The extensions to the theory include effective admittance formulas for matrix entries, incident field and reflection and transmission coefficients. The theory was verified to be correct by implementing it into a general purpose computer code and comparing its results to known solutions for waveguide phased array antennas. The new method provided a factor of five speedup in problem solution for the canonical test problems.

14. SUBJECT TERMS
Electromagnetic Fields; Scattering; Antenna Arrays; Filters; Finite Element Analysis; Computer Programs; Computational Electromagnetics; Analysis Techniques

15. NUMBER OF PAGES
46

16. PRICE CODE

17. SECURITY CLASSIFICATION OF REPORT	18. SECURITY CLASSIFICATION OF THIS PAGE	19. SECURITY CLASSIFICATION OF ABSTRACT	20. LIMITATION OF ABSTRACT
Unclassified	Unclassifed	Unclassified	UL

Standard Form 298 (Rev. 2-89) (EG)
Prescribed by ANSI Std. 239.18

TABLE OF CONTENTS

1. INTRODUCTION 1

1.1. Background and Overview 1
1.2. General Problem Description 2

2. THEORY 5

2.1. The Weak Form of the Wave Equation 5
2.2. Mode Functions and the Periodic Integral Equation 6
2.3. Periodic Radiation Boundary Terms 9
2.4. Effective Modal Admittance of One Layer 11
2.5. Effective Admittance for Multiple Layers 13
2.6. Incident Field Terms 14
2.6.1. Free Space 14
2.6.2. With Exterior Dielectric Layer 15
2.6.3. Multiple Dielectric Layers 19

2.7. Transmission and Reflection Coefficients 20
2.7.1. Free Space 21
2.7.2. With Exterior Dielectric Layer 22
2.7.3. Multiple Dielectric Layers 23

2.8. Summary of Extensions to Theory 24

3. DEMONSTRATION CASES 26

3.1. Circular Waveguide Phased Array with Dielectric Sheath 26
3.2. Rectangular Waveguide Array with Offset Dielectric Layer (Radome) . . . 28

3.2.1. Radiation 28
3.2.2. Reflection 32

4. CONCLUSIONS 34

APPENDIX A: NUMERICALLY STABLE ADMITTANCE COMPUTATION 35

REFERENCES 36

LIST OF FIGURES

1. Generic Problem Classes: (a) Phased Array Antenna with Waveguide Feeds; and (b) Planar Periodic Structure 3

2. Array Lattice Geometry and Notation 4

3. Equivalent Circuit Representation of External Dielectric Layer: (a) Geometry; (b) Transmission Line Model 11

4. Equivalent Circuit Representation for Two External Dielectric Layers: (a) Transmission Line Model; (b) Reduced Model Using Results of Section 2.4 . . . 13

5. Circular Waveguide Array: (a) Lattice Geometry; (b) Mesh of Short Waveguide Section 26

6. Comparison of Multimode [2] and HFEM Calculations for Active Reflection Coefficient of a Circular Waveguide Array with Dielectric Covers 27

7. Number of Biconjugate Gradient Iterations Needed to Solve Matrices for Cases In Figure 6 28

8. Geometry of Rectangular Waveguide Array with Air Gap and Dielectric Layer: (a) Top View; (b) Side View 29

9. Mesh Models for Rectangular Waveguide Array: (a) Unit Cell Section Above Aperture; (b) Waveguide Section Below Aperture 29

10. Active Reflection Coefficient Magnitude Calculated Using Alternative Models from Figure 9 30

11. Active Element Gain Calculated Using Alternative Models from Figure 9 31

12. Received Power (Active Element Gain) Calculated Using Alternative Models from Figure 9 for Plane Wave Incidence 33

LIST OF TABLES

I. Comparison of Size and Execution Time for Two Models of Rectangular Waveguide Array Antenna with Offset Dielectric Layer 32

1. INTRODUCTION

1.1. Background and Overview

The theory and associated software have previously been developed to compute the reflectivity and transmissivity of planar periodic structures, including active reflection coefficient of phased array antennas, using the hybrid finite element method (HFEM) with periodic boundary conditions [1]. Among its requirements was that the entire non-free-space material structure of the antenna or scatterer be contained within the finite element region, with the periodic radiation condition being applied on planar surfaces on or outside that structure. This requirement is very undesirable in a number of important circumstances in which the structure includes uniform dielectric layers. For example, consider the case of a waveguide array antenna that includes a dielectric sheath outside the array for purposes of wide-angle impedance matching, or a frequency selective surface whose outer layers are uniform dielectrics. It was previously necessary to extend the finite element mesh into the dielectric layers, with a consequent increase in the size of the matrix to be solved.

This report discusses a method for incorporating the effects of uniform external dielectric layers into the periodic radiation condition. The technique was developed previously for waveguide phased array analysis by multimode methods [2], and has also been used for frequency selective surface analysis by moment methods [3]. It is used to modify the matrix entries associated with the outermost surface of the *non-uniform* material structure by finding an effective admittance that replaces the modal admittance of the Floquet modes used to represent the exterior solution. This provides three important advantages: (1) the size of the matrix is reduced significantly, especially when the exterior layers are thick and/or dense; (2) very thin layers are permitted; and (3) it extends the range of problems that may be solved without using periodic unit-cell side wall boundary conditions that place demands on the mesh that some CAD software packages cannot satisfy. These advantages appear to come at very little cost since the only penalty is a few additional algebraic steps during the matrix fill computations.

Section 2 summarizes the original theory without exterior dielectrics and the necessary modifications. Section 3 presents calculated results with comparisons to published data obtained by other methods. Those results verify that the additions to the finite element solution are effective for both array antennas and frequency selective surfaces (FSSs).

1.2. General Problem Description

Figure 1 illustrates the two important classes of problems that this theory addresses. Fig. 1a shows a side view of an array antenna, each of whose radiating elements is fed by a single waveguide. The power incident from each waveguide is the same, but the phase may vary progressively from element to element to electronically steer the antenna beam. The answers that an array designer may require are the input impedance of an element in the array environment, called the "active impedance," the gain per element, or "active element gain," and, if grating lobes are present, the angle and power in each lobe. Accurate calculation of these quantities requires a rigorous solution that accounts for the mutual coupling between array elements. Efficient calculation relies on the assumption that the array is large, so that edge effects are negligible. When that is true, the analysis may be restricted to a single array unit cell.

Fig. 1a shows that there may be uniform dielectric layers, or "superstrates" above the non-homogeneous structure. The radiation boundary, denoted Γ_B may be placed anywhere above that part of the structure that is non-uniform. As indicated in the figure, Γ_B may cut through a dielectric, as long as that part of the dielectric above Γ_B is a continuous, planar layer.

Figure 1b shows a side view of a generic planar periodic structure. The excitation is a plane wave impinging on the lower side. The designer may need to know the amount of power reflected and transmitted, both co-polarized and cross-polarized. Also, if there are grating or Bragg lobes, their directions and relative power and phase may be important. As the figure indicates, there may be continuous dielectric layers both above and below the

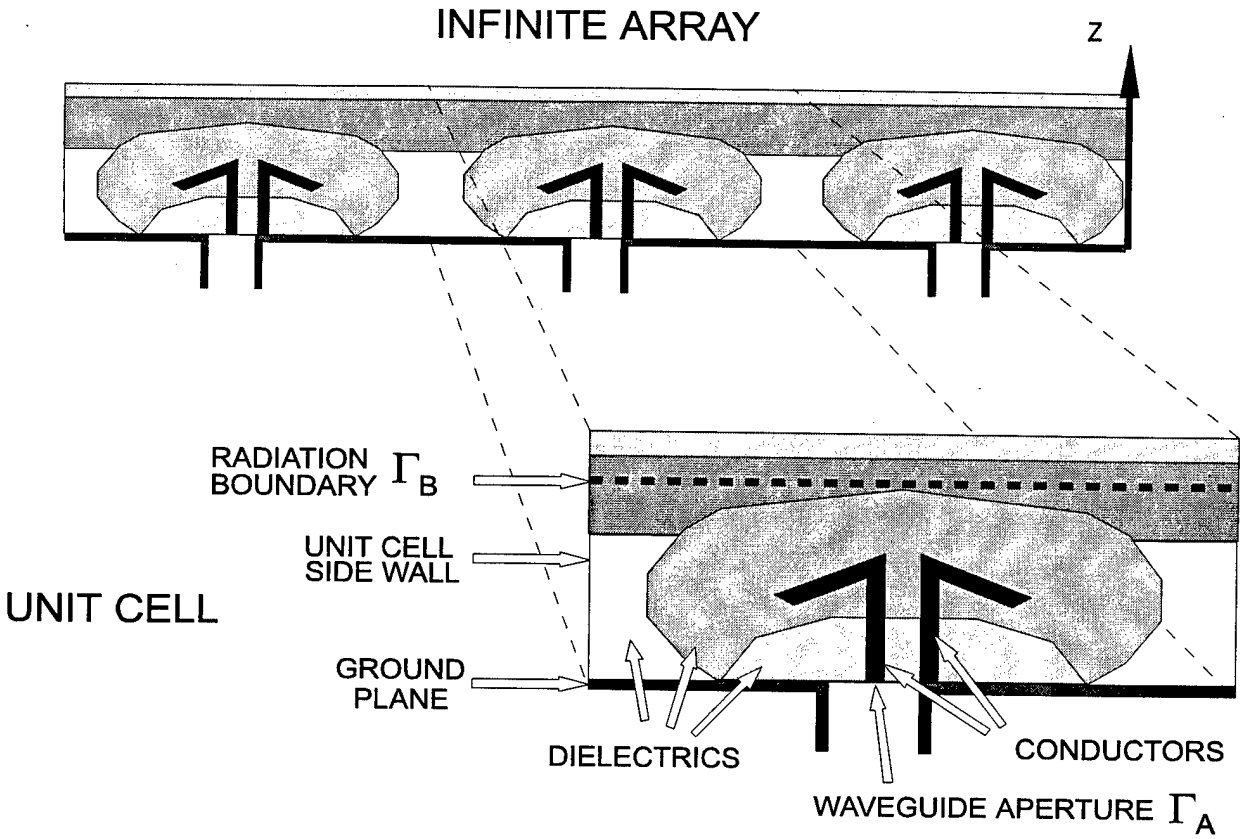

(a)

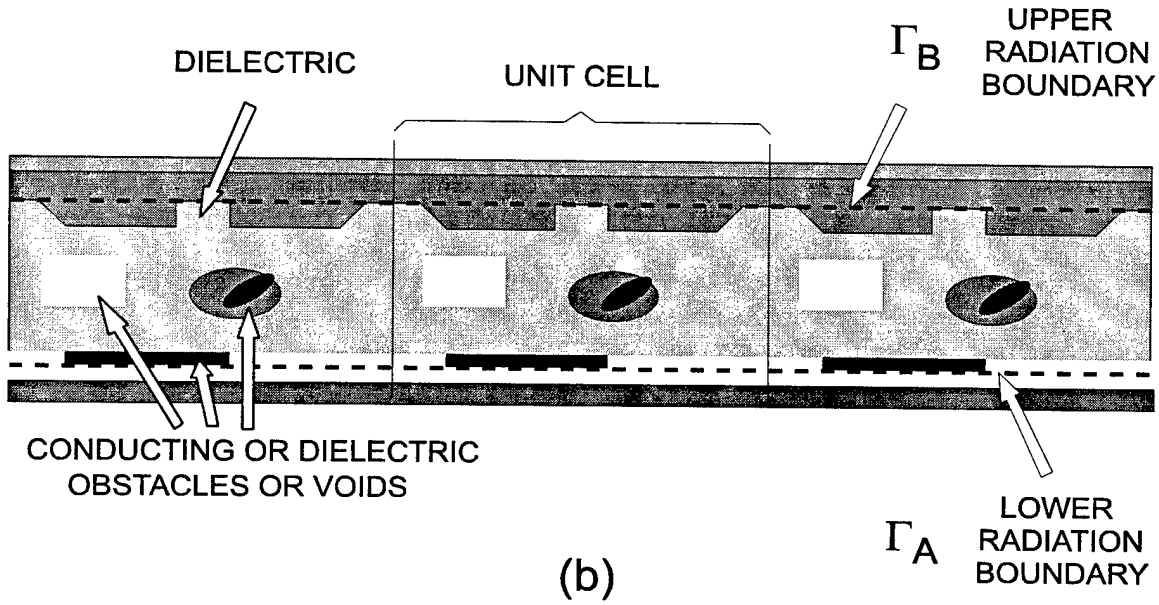

(b)

Figure 1. Generic Problem Classes: (a) Phased Array Antenna with Waveguide Feeds; and (b) Planar Periodic Structure

structure that are outside the analysis region, which is formed by the unit cell walls and the upper and lower radiation boundaries.

Figure 2 defines some of the notation used throughout this report. The structures are considered to be infinite in two directions and oriented perpendicular to the z axis. The array lattice may have an arbitrary skew angle γ. The unit cell boundary is not necessarily a parallelogram as illustrated, but may have protrusions on one side and corresponding indentations on the other, as long as the -x and +x side walls are identical except for a translation of d_x, and the -y and +y side walls are identical except for a translation of d_y in the y direction and $d_y \cot(\gamma)$ in the x direction.

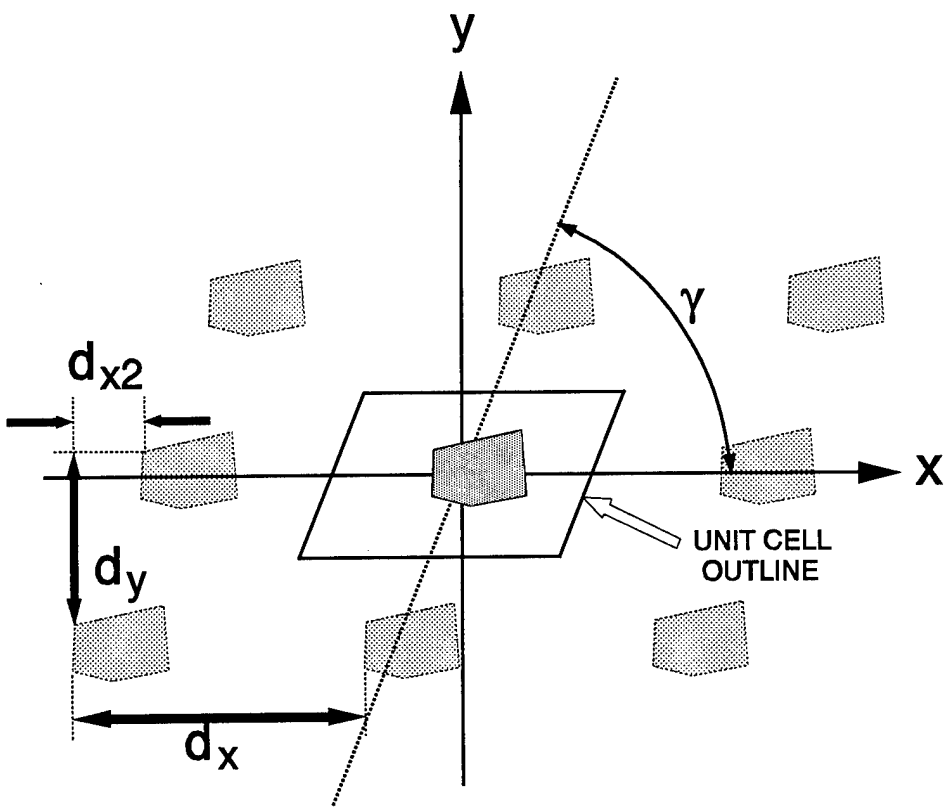

Figure 2. Array Lattice Geometry and Notation

2. THEORY

2.1. The Weak Form of the Wave Equation

The finite element solution is based on discretization of the "weak form" of the wave equation. The wave equation for the electric field in linear, isotropic, inhomogeneous media is

$$\nabla \times \frac{1}{\mu_r} \nabla \times \bar{E} - k_0^2 \epsilon_r \bar{E} = 0 \tag{1}$$

where k_0 is the free space wavenumber, and the relative permeability, μ_r, and permittivity, ϵ_r, may be functions of position. The inner product of (1) with a weighting function $\bar{W}$ is

$$\int_\Omega \bar{W}^* \cdot \left[\nabla \times \frac{1}{\mu_r} \nabla \times \bar{E} - k_0^2 \epsilon_r \bar{E} \right] dv = 0 \tag{2}$$

Using a Green's identity:

$$\int_\Omega \left[\frac{1}{\mu_r} \nabla \times \bar{W}^* \cdot \nabla \times \bar{E} - k_0^2 \epsilon_r \bar{W}^* \cdot \bar{E} \right] dv - \int_\Gamma \frac{1}{\mu_r} \bar{W}^* \times \nabla \times \bar{E} \cdot \hat{n} \, ds = 0 \tag{3}$$

where Γ is the union of all boundaries enclosing Ω as well as conducting surfaces inside Ω. Equation (3) is called the "weak form." The wave equation is satisfied in an average, or weak sense. Note that the Green's identity shifted one of the derivatives from $\bar{E}$ to $\bar{W}$, weakening the differentiability requirement on $\bar{E}$, which will permit approximation of the field with functions that only have one derivative (linear). The final form is obtained by using the Maxwell curl equation $\nabla \times \bar{E} = -j\omega\mu\bar{H}$ and the constitutive relation $\omega\mu = k_0\eta$:

$$\int_\Omega \left[\frac{1}{\mu_r} \nabla \times \bar{W}^* \cdot \nabla \times \bar{E} - k_0^2 \epsilon_r \bar{W}^* \cdot \bar{E} \right] dv - j k_0 \eta_0 \int_\Gamma \bar{W}^* \cdot (\hat{n} \times \bar{H}) \, ds = 0 \tag{4}$$

The term on the right, a surface integral over all boundaries enclosing Ω, provides the mechanism for enforcing boundary conditions. On the open parts of Γ, suitable expressions for the tangential magnetic field may be substituted to impose radiation boundary conditions. The main objective of this report is to document those expressions that are suitable for exterior dielectric layers. The expressions for the interior finite element matrix arising from the first integral in (4) are adequately described in [1] and will not be repeated here. However, the earlier derivation for the boundary terms arising from the right side integral in (4) will be reviewed because they are a necessary starting point for the present extension to the theory.

2.2. Mode Functions and the Periodic Integral Equation

The top and bottom of the unit cell are free space boundaries where a radiation condition must be applied. The method for doing so is to substitute an integral equation for $\hat{n}\times\bar{H}$ into the boundary term of the weak form. Due to the periodic nature of the problem, the integral equation may be written as a summation over "Floquet modes" [2].

Let the electric field above and below the structure be expanded in a set of mode functions $\bar{g}_{pmn}$, where the subscript p is 1 for transverse electric (i.e. $\bar{E}\perp z$) or 2 for transverse magnetic (i.e. $\bar{H}\perp z$):

$$\bar{g}_{pmn} = \bar{h}_{pmn}\, e^{j(k_{xmn}x + k_{ymn}y)} \tag{5}$$

$$\bar{h}_{1mn} = \frac{1}{\sqrt{d_x d_y}} \begin{cases} \dfrac{\left(\hat{x}\, k_{ymn} - \hat{y}\, k_{xmn}\right)}{\sqrt{k_{xmn}^2 + k_{ymn}^2}} & m,n \neq 0,0 \\ \left(\hat{x}\sin\phi_0 - \hat{y}\cos\phi_0\right) & m,n = 0,0 \end{cases} \tag{6}$$

$$\bar{h}_{2mn} = \frac{1}{\sqrt{d_x d_y}} \begin{cases} \dfrac{\left(\hat{x}\, k_{xmn} + \hat{y}\, k_{ymn}\right)}{\sqrt{k_{xmn}^2 + k_{ymn}^2}} & m,n \neq 0,0 \\ \left(\hat{x} \cos \phi_0 + \hat{y} \sin \phi_0\right) & m,n = 0,0 \end{cases} \tag{7}$$

$$k_{xmn} = k_0 \sin \theta_0 \cos \phi_0 - \frac{2\pi m}{d_x} \tag{8}$$

$$k_{ymn} = k_0 \sin \theta_0 \sin \phi_0 - \frac{2\pi n}{d_y} + \frac{2\pi m \cot \gamma}{d_x} \tag{9}$$

where (θ_0, ϕ_0) is the main beam angle, (m,n) is the mode index and γ is the lattice skew angle. The index p is 1 for modes whose electric field is transverse to z (TE), or 2 for modes whose magnetic field is transverse to z (TM). Note that the mode functions are independent of the medium's constitutive properties--the same functions will be used to represent fields in all dielectric media as well as those in free space.

At any point above the structure, the transverse electric field may be expanded in modes traveling in the $+z$ direction:

$$\bar{E}^t(z \geq 0) = \sum_{p=1}^{2} \sum_{m=-\infty}^{\infty} \sum_{n=-\infty}^{\infty} C_{pmn}^{+}\, \bar{g}_{pmn}\, e^{-j\kappa_{mn} z} \tag{10}$$

$$\kappa_{mn} = \pm \left[k_0^2 \mu_r \epsilon_r - k_{xmn}^2 - k_{ymn}^2 \right]^{1/2} \tag{11}$$

where C_{pmn}^{+} is an unknown coefficient. The sign of the propagation constant κ_{mn} is chosen as positive for outgoing waves and negative for incoming waves [2:43]. The transverse magnetic field in each mode is

$$\hat{z} \times \bar{H}^{t}_{pmn}(z \geq 0) = -Y_{pmn} \bar{E}^{t}_{pmn} \tag{12}$$

where Y_{pmn} is a modal admittance:

$$Y_{1mn} = \frac{\kappa_{mn}}{k_0 \, \eta_0 \, \mu_r} \tag{13}$$

$$Y_{2mn} = \frac{k_0 \, \epsilon_r}{\kappa_{mn} \, \eta_0} \tag{14}$$

The total magnetic field above the structure is

$$\hat{z} \times \bar{H}^{t}(z \geq 0) = -\sum_{p} \sum_{m} \sum_{n} C^{+}_{pmn} Y_{pmn} \bar{g}_{pmn} e^{-j\kappa_{mn} z} \tag{15}$$

In order to write the right side in terms of $\bar{E}^{t}$, the orthogonality property

$$\int_{unit\ cell} \bar{g}_{pmn} \cdot \bar{g}^{*}_{qij} \, dx \, dy = \delta_{pq} \, \delta_{mi} \, \delta_{nj} \tag{16}$$

is used to solve (10) for the coefficients:

$$C^{+}_{pmn} = \int_{unit\ cell} \bar{E}^{t} \cdot \bar{g}^{*}_{pmn} \, dx \, dy \tag{17}$$

with the result

$$\hat{z} \times \bar{H}^{t}(z \geq 0) = -\sum_{p} \sum_{m} \sum_{n} Y_{pmn} \bar{g}_{pmn} \int_{unit\ cell} \bar{E}^{t} \cdot \bar{g}^{*}_{pmn} \, dx \, dy \; e^{-j\kappa_{mn} z} \tag{18}$$

On the lower unit cell boundary, the transverse electric field includes an incident field

term in one of the two lowest order modes depending on whether it is transverse electric (q=1) or transverse magnetic (q=2):

$$\bar{E}^{t}(z \le 0) = \bar{g}_{q00}\, e^{-j\kappa_{00} z} + \sum_{p=1}^{2} \sum_{m=-\infty}^{\infty} \sum_{n=-\infty}^{\infty} C^{-}_{pmn}\, \bar{g}_{pmn}\, e^{j\kappa_{mn} z} \tag{19}$$

The signs of the exponential terms indicate the direction of propagation. Again, using the modes' orthogonality property,

$$C^{-}_{pmn} = \int_{unit\ cell} \bar{E}^{t} \cdot \bar{g}^{*}_{pmn}\, dx\, dy - \delta_{pq}\, \delta_{m0}\, \delta_{n0} \tag{20}$$

giving the magnetic field below the structure as

$$\hat{z} \times \bar{H}^{t}(z \le 0) = \sum_{p} \sum_{m} \sum_{n} Y_{pmn}\, \bar{g}_{pmn} \int_{unit\ cell} \bar{E}^{t} \cdot \bar{g}^{*}_{pmn}\, dx\, dy\; e^{j\kappa_{mn} z} - 2\, Y_{q00}\, \bar{g}_{q00}\, e^{-j\kappa_{00} z} \tag{21}$$

(This is a correction to eq. 37 of [1:13], which had the signs reversed.) The above expressions (18) and (21) are the integral equations that are substituted into the weak form (4) to enforce the radiation conditions. The following section derives expressions for the resulting matrix terms.

2.3. Periodic Radiation Boundary Terms

The matrix entries S^{B}_{st}, pertaining mesh edges s and t in the upper radiation boundary, are found by substituting an expansion function, $\bar{\psi}_s$(the "vector edge element"),for $\bar{E}^t$ in (18), then substituting (18) for $\hat{n} \times \bar{H}$ and $\bar{\psi}_t$ for $\bar{W}^*$ in Eq. (4):

$$S^{B}_{st} = +jk_0\, \eta_0 \int_{\Gamma_B} \bar{\psi}_t \cdot \sum_{p}\sum_{m}\sum_{n} Y_{pmn}\, \bar{g}_{pmn}\, dx\, dy \int_{\Gamma_B} [\, \bar{\psi}_s \cdot \bar{g}^{*}_{pmn}]\, dx\, dy\; e^{-j\kappa_{mn} z} \tag{22}$$

Each integral term contains a term in $\exp\{\pm j(k_{xmn}x + k_{ymn}y)\}$, which, besides the finite elements, is the only term with x or y dependence. Let $\bar{\xi}_t(k_x,k_y)$ denote the two-dimensional Fourier transform of that part of $\bar{\psi}_t$ lying on the radiation boundary:

$$\begin{aligned}\int_{\Gamma_B} \bar{\psi}_t \cdot \bar{g}_{pmn}\, dx\, dy &= \bar{h}_{pmn} \cdot \int_{\Gamma_B} \bar{\psi}_t\, e^{j(k_{xmn}x + k_{ymn}y)}\, dx\, dy \\ &= \bar{h}_{pmn} \cdot \bar{\xi}_t(k_{xmn}, k_{ymn}) \\ &= \bar{h}_{pmn} \cdot \bar{\xi}_{tmn}\end{aligned} \tag{23}$$

Now the matrix entries may be written in the more compact form

$$S^B_{st} = jk_0\eta_0 \sum_p\sum_m\sum_n \bar{\xi}_{tmn} \cdot [\, Y_{pmn}\, \bar{h}_{pmn}\, \bar{h}_{pmn}\,] \cdot \bar{\xi}^*_{smn} \tag{24}$$

Previously, an even more compact expression was obtained by summing TE and TM modes. However, when external dielectrics are present, it is important to keep those terms separate.

The expression for the matrix pertaining to the lower radiation boundary is identical to (24). This follows from the fact that the summations in (18) and (21) are the same except for the sign of the exponent inside the integral. In evaluating those integrals, the value of z in the exponent is taken as zero because it represents only a constant phase factor.

When the medium above and below the finite element region Ω is a homogenoeous dielectric half space (usually free space), (24) may be used directly. However, if the dielectric has finite thickness, or if there are multiple dielectric layers, then (24) must be modified to incorporate an <u>effective</u> modal admittance, as described in the following two sections.

2.4. Effective Modal Admittance of One Layer

Consider first a case in which the $+z$ radiation boundary (Γ_B) is covered by a single dielectric sheet. Let Y' denote the effective admittance of any Floquet mode propagating in the $+z$ direction through the sheet, whose admittance for that mode is Y^M. (The subscripts for mode indices are dropped in the following derivation since it applies equally to all modes. The superscript A denotes air, while M denotes material.) At distance t beyond the reference point, the slab terminates at a half space whose admittance is Y^A (free space). Figure 3 is an equivalent circuit depiction using a transmission line analogy. The reflection coefficient at the $z = t$ boundary due to the admittance mismatch is

$$\rho = \frac{Y^A - Y^M}{Y^A + Y^M} \tag{25}$$

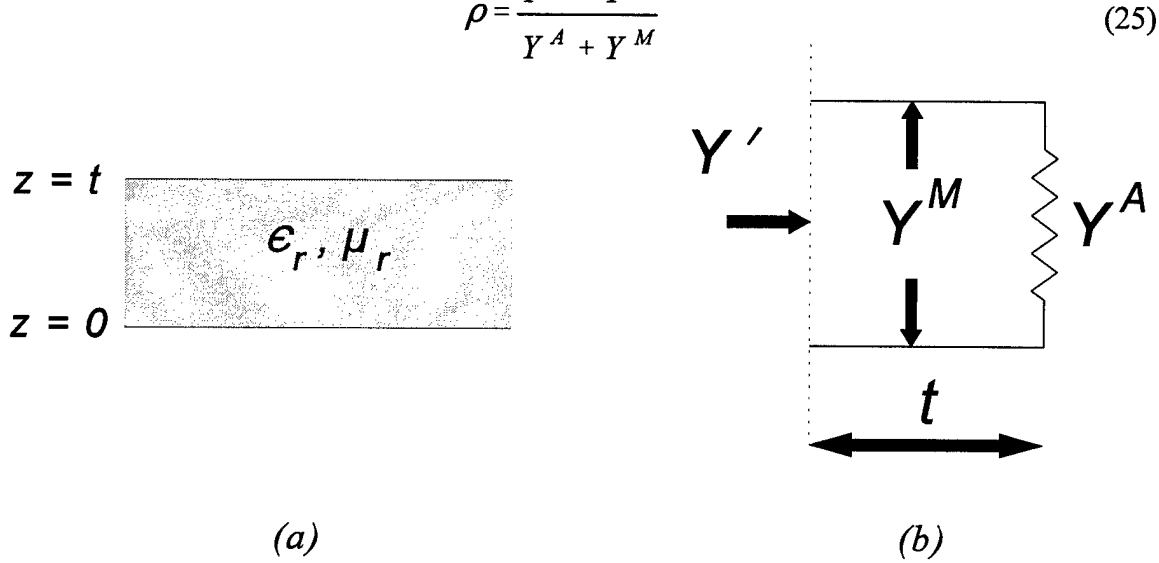

Figure 3. Equivalent Circuit Representation of External Dielectric Layer:
(a) Geometry; (b) Transmission Line Model

Y′ is the ratio $\bar{H} / \bar{E}$ at the reference point. The electric and magnetic fields carried by the mode are (normalized to the field strength of the $+z$ component at $z = 0$):

$$\bar{E} = e^{-j\kappa^M z} - \rho e^{-j\kappa^M (z+2t)} \tag{26}$$

$$\bar{H} = Y^M \left[e^{j\kappa^M z} + \rho e^{-j\kappa^M (z+2t)} \right] \tag{27}$$

where κ^M is the z-directed propagation constant for the mode from (11). The first term in each of (26) and (27) represents the wave traveling in the $+z$ direction, while the second term represents the reflected wave traveling in the $-z$ direction. Taking the ratio of magnetic to electric field at $z = 0$ and multiplying the numerator and denominator by $\exp\{j\,\kappa^M t\}$:

$$Y' = Y^M \frac{e^{j\kappa^M t} + \rho e^{-j\kappa^M t}}{e^{j\kappa^M t} - \rho e^{-j\kappa^M t}} \tag{28}$$

which is the usual expression for an admittance discontinuity transformed back a distance t along a uniform transmission line whose characteristic admittance is Y^M [4:10]. A more convenient expression is obtained using the Euler identities:

$$Y' = Y^M \frac{\cos(\kappa^M t) + j\left(Y^M / Y^A\right)\sin(\kappa^M t)}{\left(Y^M / Y^A\right)\cos(\kappa^M t) + j\sin(\kappa^M t)} \tag{29}$$

An important feature of Floquet modes, like any waveguide modes that can be expressed in terms of orthogonal transverse mode functions, is that any discontinuity transverse to the direction of propagation (z in this case) does not cause cross-coupling between modes. The (m,n) mode incident on a dielectric boundary parallel to the x-y plane will reflect energy only into the (m,n) mode in the dielectric, and transmit energy only in the (m,n) mode in free space. Consequently, the earlier expression for boundary matrix entries, Eq. (24) may be modified simply by replacing Y_{pmn} with

$$Y_{pmn} \leftarrow Y^M_{pmn} \frac{\cos(\kappa^M_{mn} t) + j\left(Y^M_{pmn} / Y^A_{pmn}\right)\sin(\kappa^M_{mn} t)}{\left(Y^M_{pmn} / Y^A_{pmn}\right)\cos(\kappa^M_{mn} t) + j\sin(\kappa^M_{mn} t)} \tag{30}$$

where Y_{mn}^{M} and Y_{mn}^{A} denote the modal admittances in uniform media, dielectric and free space, respectively.

Some caution is needed in calculating (30) numerically because the complex sine and cosine involve sinh and cosh functions. For large m and n, κ_{mn} is a large complex number and may cause floating point overflow in those function evaluations. Appendix A describes a stable approach to evaluating (30) that avoids the problem.

2.5. Effective Admittance for Multiple Layers

Consider next a case in which there are two exterior dielectric layers, with the innermost having a thickness t_2 and characteristic modal admittance Y^{M2}. Figure 4(a) shows a transmission line analogy for this situation. The second (outermost) layer is identical to the one considered in the previous section. Noting that the portion of the circuit to the right of the second dotted line is identical to that shown earlier in Fig. 3, the reduced model shown in Fig. 4(b) is equivalent. Now, noting the similarity of Fig. 3(b) to Fig. 4(b), it is evident that Y'' is given by Eq. (30) with the substitutions $\kappa^{M} \leftarrow \kappa^{M2}$, $Y^{M} \leftarrow Y^{M2}$, and $Y^{A} \leftarrow Y'$. By extension, Eq. (30) can be used as a recursion formula for any number of layers.

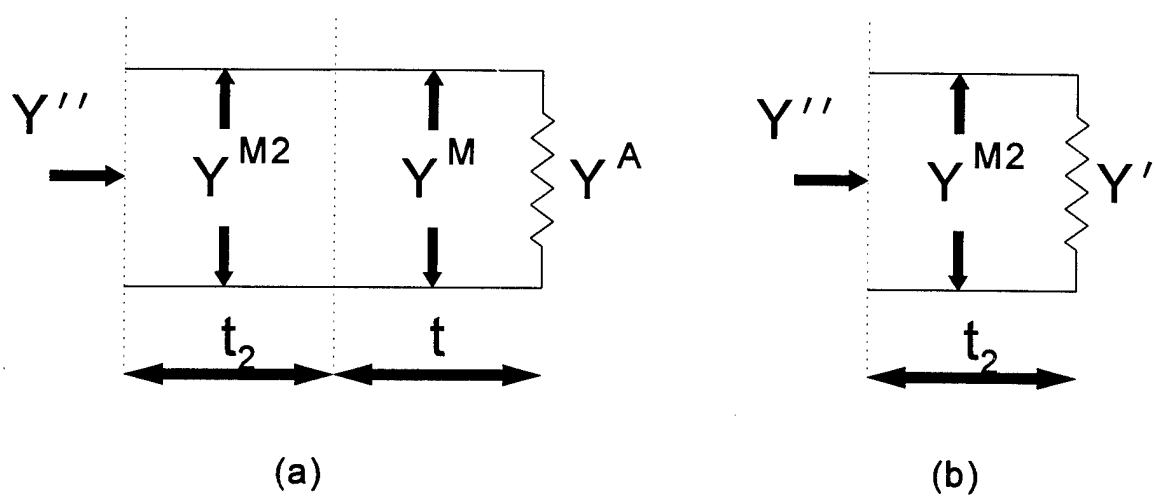

Figure 4. Equivalent Circuit Representation for Two External Dielectric Layers: (a) Transmission Line Model; (b) Reduced Model Using Results of Section 2.4

2.6. Incident Field Terms

2.6.1. Free Space

The right side vector in the matrix equation arises from the second term on the right side of (21), due to a unit amplitude incident electric field arriving from $z < 0$. Its form is a plane wave, which is the 0,0-order Floquet mode. The vector entry for edge t is:

$$e_t^{inc} = -j\, k_0\, \eta_0 \int_{\Gamma_A} \bar{\Psi}_t \cdot (2\, Y_{q00}\, \bar{g}_{q00})\, dx\, dy \tag{31}$$

The constant phase factor $\exp\{-j\, \kappa_{mn}\, z\}$ in (21) is ignored. Taking all of the terms outside the integral that do not depend on x and y:

$$e_t^{inc} = -2j\, k_0\, \eta_0\, Y_{q00}\, \bar{h}_{q00} \cdot \int_{\Gamma_A} \bar{\Psi}_t\, e^{j(k_{x00}x + k_{y00}y)}\, dx\, dy \tag{32}$$

Note that the integral is the two-dimensional Fourier transform of the finite element's tangential component on Γ_A, which is denoted $\bar{\xi}_{t00}$. Note also the following simplification from (8) and (9):

$$k_{x00}^2 + k_{y00}^2 = k_0^2 \sin^2\theta_0 \tag{33}$$

When the medium is free space, the dominant mode admittance is then

$$Y_{q00} = \begin{cases} \dfrac{\cos\theta_0}{\eta_0} & q = 1 \\[2ex] \dfrac{1}{\eta_0 \cos\theta_0} & q = 2 \end{cases} \tag{34}$$

Now (32) may be rewritten in the form

$$e_t^{inc} = \frac{-2j\,k_0}{\sqrt{d_x\,d_y}} \begin{cases} \cos\theta_0\,(\hat{x}\sin\phi_0 - \hat{y}\cos\phi_0)\cdot\bar{\xi}_{t00} & q=1 \\ \sec\theta_0\,(\hat{x}\cos\phi_0 + \hat{y}\sin\phi_0)\cdot\bar{\xi}_{t00} & q=2 \end{cases} \tag{35}$$

2.6.2. With Exterior Dielectric Layer

For the case in which there is a dielectric layer covering the side of a periodic structure on which an incident wave impinges, the incident field admittance term Y_{q00} in (21) will be different than (34). To determine the correct form, modal expansions for the fields in and outside the dielectric will be matched at the air-dielectric interface, then the ratio $Y' = (\hat{z}\times\bar{H}) / \bar{E}$ will be evaluated at $z = 0$ for each mode. In the following analysis, the finite element domain will be assumed to occupy part of the region $z \geq 0$, while the dielectric slab occupies the region $-t \leq z \leq 0$.

In the free space region $z \leq -t$, the transverse electric field is again represented by a unit-amplitude wave in the 0`th order Floquet mode traveling in the $+z$ direction, and some unknown number of modes with unknown weights C_{pmn}, traveling in the $-z$ direction:

$$\bar{E}^t(z \leq -t) = \bar{g}_{q00}\,e^{-j\kappa_{00}(z+t)} + \sum_{p,m,n} C_{pmn}\,\bar{g}_{pmn}\,e^{j\kappa_{mn}(z+t)} \tag{36}$$

which is the same as (19) except that the phase reference is now the air-dielectric interface (the limits on summations over p, m and n are the same as in (19). The corresponding magnetic field is

$$\begin{aligned} \hat{z}\times\bar{H}^t(z \leq -t) = & -Y_{q00}\,\bar{g}_{q00}\,e^{-j\kappa_{00}(z+t)} \\ & + \sum_{p,m,n} Y_{pmn}\,C_{pmn}\,\bar{g}_{pmn}\,e^{j\kappa_{mn}(z+t)} \end{aligned} \tag{37}$$

In the dielectric region, it is not adequate to represent the $+z$ traveling wave as the incident mode only because it may include other modes scattered from $z \geq 0$, then reflected by the dielectric interface at $z = -t$. Hence, the transverse fields in the dielectric are comprised of an unknown number of modes traveling in each direction:

$$\bar{E}^{t}(-t \leq z \leq 0) = \sum_{p,m,n} \bar{g}_{pmn}(A_{pmn}\, e^{-j\kappa_{mn}^{M} z} + B_{pmn}\, e^{j\kappa_{mn}^{M} z}) \tag{38}$$

$$\hat{z} \times \bar{H}^{t}(-t \leq z \leq 0) = -\sum_{p,m,n} Y_{pmn}^{M}\, \bar{g}_{pmn}(A_{pmn}\, e^{-j\kappa_{mn}^{M} z} - B_{pmn}\, e^{j\kappa_{mn}^{M} z}) \tag{39}$$

The phase reference for the fields in the dielectric is at z = 0, while that for the fields in free space given by (36) and (37) is at $z = -t$. This constant phase difference is absorbed into the complex constants A_{pmn} and B_{pmn}.

Equating (36) and (38) at $z = -t$, then taking the product with each mode function and integrating over the unit cell cross section, the following result arises due to the orthogonality of modes:

$$\delta_{pq}\,\delta_{m0}\,\delta_{n0} + C_{pmn} = A_{pmn}\, e^{j\kappa_{mn}^{M} t} + B_{pmn}\, e^{-j\kappa_{mn}^{M} t} \tag{40}$$

Equating components from (37) and (39):

$$Y_{pmn}(\delta_{pq}\,\delta_{m0}\,\delta_{n0} - C_{pmn}) = Y_{pmn}^{M}(A_{pmn}\, e^{j\kappa_{mn}^{M} t} - B_{pmn}\, e^{-j\kappa_{mn}^{M} t}) \tag{41}$$

Combining (40) and (41) leads to an expression for $(A_{pmn} - B_{pmn})$ in terms of $(A_{pmn} + B_{pmn})$ as follows:

$$A_{pmn} e^{j\kappa_{mn}^{M} t} + B_{pmn} e^{-j\kappa_{mn}^{M} t} = 2\,\delta_{pq}\,\delta_{m0}\,\delta_{n0} - \frac{Y_{pmn}^{M}}{Y_{pmn}} \left(A_{pmn} e^{j\kappa_{mn}^{M} t} - B_{pmn} e^{-j\kappa_{mn}^{M} t} \right) \tag{42}$$

$$\begin{aligned} Y_{pmn}\Big[(A_{pmn} + B_{pmn}) \cos(\kappa_{mn}^{M} t) + j(A_{pmn} - B_{pmn}) \sin(\kappa_{mn}^{M} t) \Big] = \\ -Y_{pmn}^{M}\Big[(A_{pmn} - B_{pmn}) \cos(\kappa_{mn}^{M} t) + j(A_{pmn} + B_{pmn}) \sin(\kappa_{mn}^{M} t) \Big] \\ + 2\, Y_{pmn}\, \delta_{pq}\, \delta_{m0}\, \delta_{n0} \end{aligned} \tag{43}$$

$$\begin{aligned} (A_{pmn} - B_{pmn}) \Big(Y_{pmn}^{M} \cos(\kappa_{mn}^{M} t) + j\, Y_{pmn} \sin(\kappa_{mn}^{M} t) \Big) = \\ 2\, Y_{pmn}\, \delta_{pq}\, \delta_{m0}\, \delta_{n0} - (A_{pmn} + B_{pmn}) \Big(Y_{pmn} \cos(\kappa_{mn}^{M} t) + j\, Y_{pmn}^{M} \sin(\kappa_{mn}^{M} t) \Big) \end{aligned} \tag{44}$$

$$\begin{aligned} (A_{pmn} - B_{pmn}) = & \frac{2\, Y_{q00}}{Y_{q00}^{M} \cos(\kappa_{00}^{M} t) + j\, Y_{q00} \sin(\kappa_{00}^{M} t)} \\ & - (A_{pmn} + B_{pmn}) \frac{Y_{pmn} \cos(\kappa_{mn}^{M} t) + j\, Y_{pmn}^{M} \sin(\kappa_{mn}^{M} t)}{Y_{pmn}^{M} \cos(\kappa_{mn}^{M} t) + j\, Y_{pmn} \sin(\kappa_{mn}^{M} t)} \end{aligned} \tag{45}$$

Referring back to (39), the transverse magnetic field evaluated at $z = 0$ is

$$\hat{z} \times \bar{H}^{t} \Big|_{z=0} = - \sum_{p,m,n} Y_{pmn}^{M}\, \bar{g}_{pmn} (A_{pmn} - B_{pmn}) \tag{46}$$

The integral equation for the magnetic field in the region $z \le 0$ is

$$\hat{z} \times \bar{H}^{t}(z \le 0) = \sum_{p,m,n} Y'_{pmn}\, \bar{g}_{pmn} \int_{unit\ cell} \bar{E}^{t} \cdot \bar{g}^{*}_{pmn}\, dx\, dy\; e^{j \kappa^{M}_{mn} z} - 2\, \tilde{Y}'_{q00}\, \bar{g}_{q00}\, e^{-j \kappa^{M}_{00} z} \tag{47}$$

Note the primes on the admittances, denoting that these are now effective admittances. In addition, the tilde over Y in the second term on the right distinguishes the incident field admittance. Evaluating (47) at $z = 0$ with $\bar{E}^{t}$ from (38):

$$\hat{z} \times \bar{H}^{t} \Big|_{z=0} = -2\, \tilde{Y}'_{q00}\, \bar{g}_{q00} + \sum_{p,m,n} Y'_{pmn}\, \bar{g}_{pmn} (A_{pmn} + B_{pmn}) \tag{48}$$

Equating this to (46) gives:

$$\sum_{p,m,n} Y^{M}_{pmn}\, \bar{g}_{pmn} (A_{pmn} - B_{pmn}) = 2\, \tilde{Y}'_{q00} - \sum_{p,m,n} Y'_{pmn}\, \bar{g}_{pmn} (A_{pmn} + B_{pmn}) \tag{49}$$

and exploiting the modes' orthogonality again:

$$(A_{pmn} - B_{pmn}) = 2\, \frac{\tilde{Y}'_{q00}}{Y^{M}_{pmn}}\, \delta_{pq}\, \delta_{m0}\, \delta_{n0} - \frac{Y'_{pmn}}{Y^{M}_{pmn}} (A_{pmn} + B_{pmn}) \tag{50}$$

Comparing this to (45) it is now evident that the equivalent admittance for the incident field term is

$$\tilde{Y}'_{q00} = \frac{Y_{q00}\, Y^{M}_{q00}}{Y^{M}_{q00} \cos(\kappa^{M}_{00} t) + j\, Y_{q00} \sin(\kappa^{M}_{00} t)} \tag{51}$$

which is to be substituted for Y_{q00} in (32). The earlier comment regarding the sign of κ_{mn} from (11) is especially important here, because it will result in a sign change in the second denominator term.

2.6.3. Multiple Dielectric Layers

Suppose now that there is a second dielectric layer occupying the space $0 \le z \le t_2$, and the boundary Γ_A is at $z = t_2$. The finite element domain is now in the region $z \ge t_2$. The fields in the second dielectric layer may be expressed as in (38) and (39), except with the phase reference at $z = t_2$:

$$\bar{E}^t(0 \le z \le t_2) = \sum_{p,m,n} \bar{g}_{pmn}\left(a_{pmn}\, e^{-j\kappa_{mn}^{M2}(z-t_2)} + b_{pmn}\, e^{j\kappa_{mn}^{M2}(z-t_2)} \right) \tag{52}$$

$$\hat{z} \times \bar{H}^t(0 \le z \le t_2) = -\sum_{p,m,n} Y_{pmn}^{M2}\, \bar{g}_{pmn}\left(a_{pmn}\, e^{-j\kappa_{mn}^{M2}(z-t_2)} - b_{pmn}\, e^{j\kappa_{mn}^{M2}(z-t_2)} \right) \tag{53}$$

Matching fields at $z = 0$ with (38) and (39) and applying mode orthogonality gives

$$(A_{pmn} + B_{pmn}) = (a_{pmn}\, e^{-j\kappa_{mn}^{M2} t_2} + b_{pmn}\, e^{j\kappa_{mn}^{M2} t_2}) \tag{54}$$

$$Y_{pmn}^{M}(A_{pmn} - B_{pmn}) = Y_{pmn}^{M2}(a_{pmn}\, e^{-j\kappa_{mn}^{M2} t_2} - b_{pmn}\, e^{j\kappa_{mn}^{M2} t_2}) \tag{55}$$

Combining the above two with (50):

$$
\begin{aligned}
2\,\tilde{Y}^{/}_{q00}\,\delta_{pq}\,\delta_{m0}\,\delta_{n0} - Y^{/}_{pmn}\,(a_{pmn}\,e^{-j\kappa^{M2}_{mn}t_2} + b_{pmn}\,e^{j\kappa^{M2}_{mn}t_2}) \\
= Y^{M2}_{pmn}\,(a_{pmn}\,e^{-j\kappa^{M2}_{mn}t_2} - b_{pmn}\,e^{j\kappa^{M2}_{mn}t_2})
\end{aligned}
\tag{56}
$$

which may be solved for $(a_{pmn} - b_{pmn})$ in terms of $(a_{pmn} + b_{pmn})$ with the result:

$$
\begin{aligned}
(a_{pmn} - b_{pmn}) = & \frac{2\,\tilde{Y}^{/}_{q00}}{Y^{M2}_{q00}\cos(\kappa^{M2}_{00}t_2) + j\,Y^{/}_{q00}\sin(\kappa^{M2}_{00}t_2)} \\
& - (a_{pmn} + b_{pmn})\,\frac{Y^{/}_{pmn}\cos(\kappa^{M2}_{mn}t_2) + j\,Y^{M2}_{pmn}\sin(\kappa^{M2}_{mn}t_2)}{Y^{M2}_{pmn}\cos(\kappa^{M2}_{mn}t_2) + j\,Y^{/}_{pmn}\sin(\kappa^{M2}_{mn}t_2)}
\end{aligned}
\tag{57}
$$

Note the distinction between $\tilde{Y}'$ in the numerator and Y' in the denominator. The former is the incident field equivalent admittance computed using (51). The latter is due to the transformed surface discontinuity from (30). The sign of κ_{00} is negative since it is due to an incoming wave. The same is true for the computation of Y'_{00} in the denominator of the first term--consequently it will be the complex conjugate of the corresponding Y'_{00} in the second term. With those caveats, the equivalent admittance for the incident field arriving at Γ_A through a second layer is

$$
\tilde{Y}^{//}_{q00} = \frac{\tilde{Y}^{/}_{q00}\,Y^{M2}_{q00}}{Y^{M2}_{q00}\cos(\kappa^{M2}_{00}t_2) + j\,Y^{/}_{q00}\sin(\kappa^{M2}_{00}t_2)}
\tag{58}
$$

2.7. Transmission and Reflection Coefficients

The two types of analyses shown in Figure 1, array antennas and periodic screens, give rise to two types of reflection terms: waveguide mode and Floquet mode. Waveguide reflection terms are computed in the same way regardless of whether there are superstrate

layers. Those waveguide terms are discussed adequately in [5] and [6]. The following derivations apply to the free-space Floquet mode transmission terms for both analysis types, as well as the reflection terms for periodic screens.

2.7.1. Free Space

The excitation coefficients C_{pmn} for Floquet modes above the structure (in the $z > 0$ halfspace) are given by (17) as the products of the transverse field on Γ_B and the mode function, integrated over the unit cell cross section. These are proportional to the transmission coefficients: when the incident and transmitted modes are different, the square root of their admittance ratio must be included. Let τ^+_{pmn} denote the transmission coefficient in the $+z$ direction for mode p,m,n:

$$\tau^+_{pmn} = \sqrt{\frac{Y_{pmn}}{Y_{inc}}} \sum_{s \in \Gamma_B} e_s \, \bar{\xi}^*_{smn} \cdot \bar{h}_{pmn} \tag{59}$$

The summation is an approximation to the integral in (17), with the electric field approximated using finite elements. For antenna radiation, Y_{inc} is the admittance of a waveguide mode. For periodic screen reflection *and* transmission it is the admittance of the 0,0-order Floquet mode *in free space*.

For periodic screens, the modal excitation coefficients for waves reflected into the $-z$ half space are given by (20). The reflection coefficients τ^-_{pmn} for all except the lowest order mode are given by (59) with Γ_A replacing Γ_B. The lowest order coefficient, the reflectivity is

$$\tau^-_{p00} = \sqrt{\frac{Y_{p00}}{Y_{q00}}} \left[\sum_{s \in \Gamma_A} \left(e_s \, \bar{\xi}^*_{s00} \cdot \bar{h}_{p00} \right) - \delta_{pq} \right] \tag{60}$$

where q represents the incident wave polarization.

2.7.2 With Exterior Dielectric Layer

The reflection and transmission coefficients must be found from the inner products of the mode functions with the transverse fields over the boundaries Γ_A and Γ_B although the desired response is that measured outside the exterior dielectrics. The modal excitation coefficients are the C_{pmn}'s in (36) and (37), and it is necessary to relate them to the inner products calculated in terms of A_{pmn} and B_{pmn}. If (38) is evaluated at $z = 0$ and then the inner products of both sides with each mode function are taken, the result is

$$\left(A_{pmn} + B_{pmn}\right) = \int_{unit\ cell} \bar{E}^{t} \cdot \bar{g}^{*}_{pmn}\, dx\, dy \tag{61}$$

Since the existing computer code calculates the inner product on the right, all that is necessary now is to find C_{pmn} in terms of $(A_{pmn}+B_{pmn})$. Rewriting (40):

$$C_{pmn} = \cos(\kappa^{M}_{mn} t)\,(A_{pmn} + B_{pmn}) + j\sin(\kappa^{M}_{mn} t)\,(A_{pmn} - B_{pmn}) - \delta_{pq}\,\delta_{m0}\,\delta_{n0} \tag{62}$$

The reflected and transmitted terms only from (50) are:

$$(A_{pmn} - B_{pmn}) = -\frac{Y^{/}_{pmn}}{Y^{M}_{pmn}}\,(A_{pmn} + B_{pmn}) \tag{63}$$

and substituting (29) and (63) into (62) leads to

$$C_{pmn} = -\delta_{pq}\,\delta_{m0}\,\delta_{n0} + (A_{pmn} + B_{pmn})\,\frac{Y^{M}_{pmn}}{Y^{M}_{pmn}\cos(\kappa^{M}_{mn} t) + j\,Y_{pmn}\sin(\kappa^{M}_{mn} t)} \tag{64}$$

which is the desired result. Therefore, the reflection coefficients for the -z half space are

$$\tau^{-}_{pmn} = \sqrt{\frac{Y_{pmn}}{Y_{inc}}} \left[y'_{pmn} \sum_{s \in \Gamma_A} e_s \, \bar{\xi}^{*}_{smn} \cdot \bar{h}_{pmn} - \delta_{pq} \, \delta_{m0} \, \delta_{n0} \right] \tag{65}$$

where y'_{pmn} is the admittance *ratio* appearing on the right side of (64):

$$y'_{pmn} = \left[\cos(\kappa^{M}_{mn} t) + j \frac{Y_{pmn}}{Y^{M}_{pmn}} \sin(\kappa^{M}_{mn} t) \right]^{-1} \tag{66}$$

The incident mode admittance, Y_{inc}, is the free space modal admittance, as given by (35). The transmission coefficients for the +z half space are also given by (59), without the Kronecker delta term due to the incident field.

2.7.3. Multiple Dielectric Layers

Extension of the above to multiple layers is not a straightforward matter of using (66) recursively. Instead, the formula must be derived by matching fields across a second boundary in a similar manner to Section 2.6.3.

Let the fields in the innermost of two layers be represented as in (52) and (53). Then matching fields across the boundary between the two dielectric layers gives (54), which may be substituted into (64) to give

$$C_{pmn} = -\delta_{pq} \, \delta_{m0} \, \delta_{n0} + y'_{pmn} \left(a_{pmn} e^{j \kappa^{M2}_{mn} t_2} + b_{pmn} e^{-j \kappa^{M2}_{mn} t_2} \right) \tag{67}$$

Expanding the complex exponentials gives a form similar to (62):

$$C_{pmn} = -\delta_{pq}\delta_{m0}\delta_{n0} + y'_{pmn}\left[\cos(\kappa^{M2}_{mn} t_2)(a_{pmn} + b_{pmn}) + j\sin(\kappa^{M2}_{mn} t_2)(a_{pmn} - b_{pmn})\right] \tag{68}$$

By analogy from (63), $(a_{pmn} - b_{pmn})$ in terms of $(a_{pmn} + b_{pmn})$ is

$$(a_{pmn} - b_{pmn}) = -\frac{Y''_{pmn}}{Y^{M2}_{pmn}}(a_{pmn} + b_{pmn}) \tag{69}$$

and substitution of this along with (30) using the recursion substitutions from Section 2.5 into (68) gives

$$C_{pmn} = -\delta_{pq}\delta_{m0}\delta_{n0} + (a_{pmn} + b_{pmn})\, y'_{pmn} \frac{Y^{M2}_{pmn}}{Y^{M2}_{pmn}\cos(\kappa^{M2}_{mn} t_2) + j\, Y'_{pmn}\sin(\kappa^{M2}_{mn} t_2)} \tag{70}$$

where Y'_{pmn} is computed according to (29). This is the necessary form, giving the coefficients C_{pmn} in terms of $(a_{pmn} + b_{pmn})$, which take the place of $(A_{pmn} + B_{pmn})$ in the inner product of (47). The quotient in (70) is a second admittance ratio, which may be denoted y''_{pmn}. Thus, the approach for transmission and reflection coefficients for multiple layers is not to use a formula recursively, but to multiply their admittance ratios together.

2.8. Summary of Extensions to Theory

The most general case in terms of the foregoing, the one that embodies all elements of the extensions to theory, is a periodic screen that has external dielectrics on both sides. To solve for the properties of such a structure, the following extensions to the theory need to be incorporated in the computer code:

A. In computing the matrix entries associated with Γ_A and Γ_B, the equivalent

admittance from (30) is used in place of the admittance in (24). This effective admittance represents the reflection coefficient for a Floquet mode transformed back to the radiation boundary through the dielectric(s).

B. In computing the right hand side terms for Γ_A, an equivalent admittance from (51) or (58) is used in place of the admittance in (32). This effective admittance represents the modal admittance of the incident field transformed forward through the dielectric(s).

C. In computing the power reflection and transmission from the fields (determined by solving the matrix equation), the admittance ratio from (66) must be included. This accounts for a transformation of the Floquet mode admittance back through the dielectric(s) to the integration surface where the field solution is available.

For array radiation analyses, step (B) is skipped and (A) and (C) are carried out for Γ_B only. For array reflection, all three steps are also required.

This completes the presentation of theoretical derivations. The following chapter presents test cases used to verify the above formulas.

3. DEMONSTRATION CASES

3.1. Circular Waveguide Phased Array with Dielectric Sheath

Figure 5(a) shows the geometry of an array of circular waveguides that open into free space through a ground plane. There may also be a dielectric layer just outside the waveguide openings. Figure 5(b) is a view of the finite element model, which represents a short section of a single waveguide just below the ground plane. Waveguide mode boundary conditions are imposed on the -*z* side to simulate the effect of an arbitrarily-long, match-terminated waveguide as discussed in [5] and [6]. The incident field carried by the waveguides is in the TE_{11} mode, polarized in the y direction (q=2). The periodic radiation condition discussed in section 2.3 is imposed on the +*z* side.

Figure 6 compares HFEM calculations with multimode results from Amitay [2:299] for the active reflection coefficient magnitude for scanning in the E plane ($\phi = 90°$). The three solid curves are the multimode results for slab thicknesses of 0, .1 λ, and .5 λ. The three sets of discrete points are the corresponding HFEM results. The fact that the two results agree so closely confirms the validity of the expressions derived for the radiation

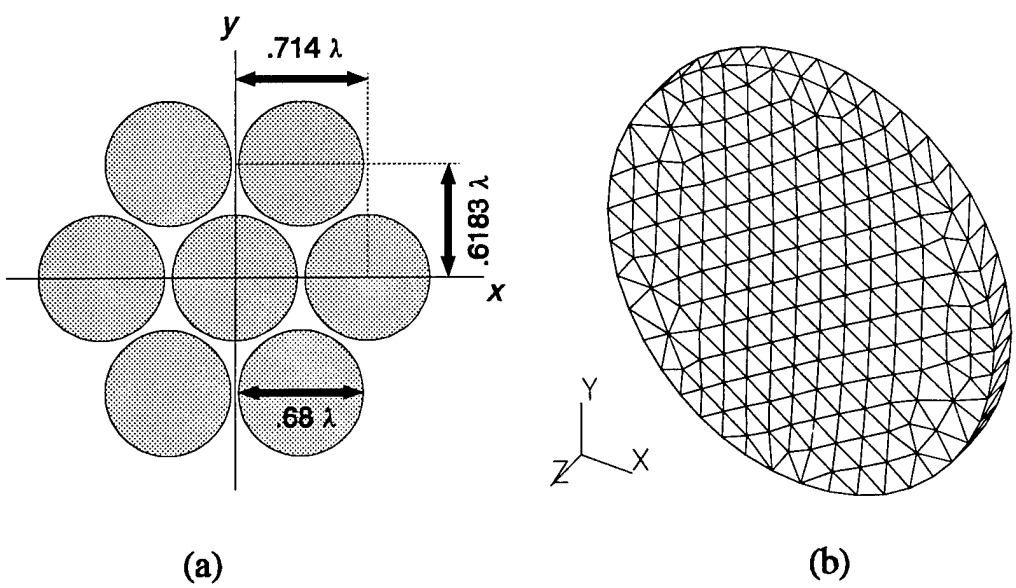

Figure 5. Circular Waveguide Array: (a) Lattice Geometry;
(b) Mesh of Short Waveguide Section

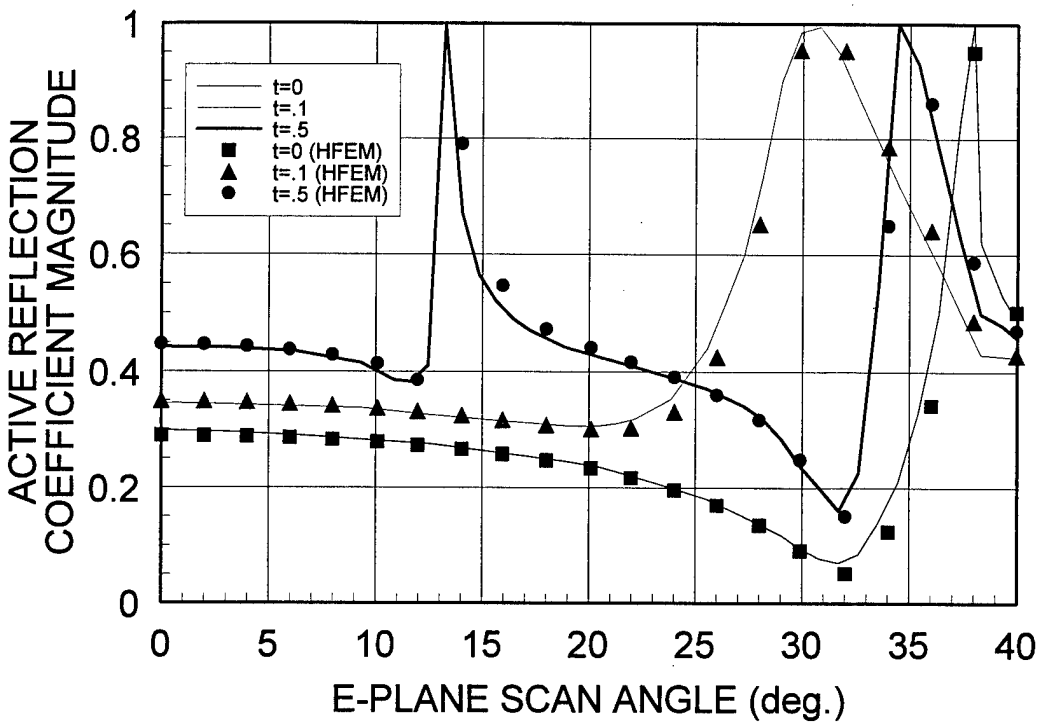

Figure 6. Comparison of Multimode [2] and HFEM Calculations for Active Reflection Coefficient of a Circular Waveguide Array with Dielectric Covers

boundary matrix, specifically, the effective admittance given by (30). This test case also validated the accuracy of the equivalent admittance (66) used for computing the transmission and reflection coefficients because the total power transmitted into all propagating Floquet modes plus that reflected back into the waveguide summed to unity for all angles.

Figure 7 shows the number of iterations required to solve the matrix in each of the three cases from Figure 6 using the biconjugate gradient method (BCGM) [7]. Consistent with prior experience, the number of iterations increases near scan blindnesses. Otherwise, it is nearly the same for all three cases. The addition of the exterior dielectric has very little effect on convergence, and therefore very little effect on the matrix condition number. This substantiates the claim made in the introduction that the additional capability for external dielectrics comes at almost no added cost in solution time.

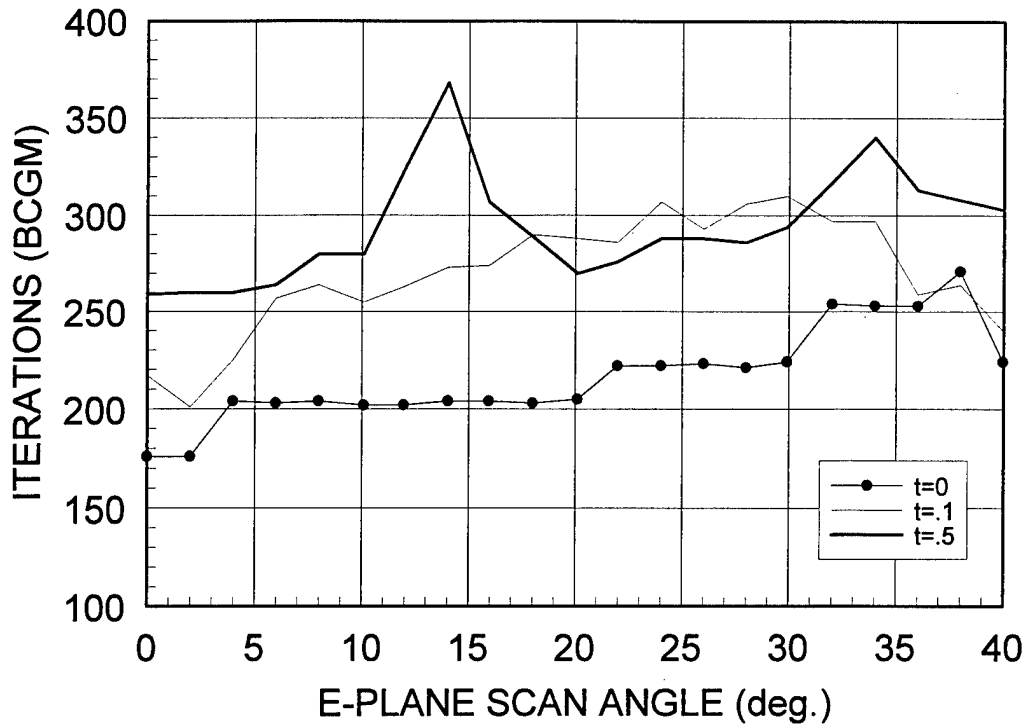

Figure 7. Number of Biconjugate Gradient Iterations Needed to Solve Matrices for Cases in Figure 6

3.2. Rectangular Waveguide Array with Offset Dielectric Layer (Radome)

3.2.1. Radiation

Figure 8 shows the geometry of an array of open-ended rectangular waveguides with an air gap between the ground plane and a dielectric layer, representing an antenna with a radome, and an air gap between the radome and the radiating aperture.

Figure 9 shows the grids for two unit cell models to contrast the ways HFEM can be used to analyze the radiation from this array. In the first, Fig. 9a, the mesh model represents a section of a unit cell outside the waveguide opening, including both the air gap and the

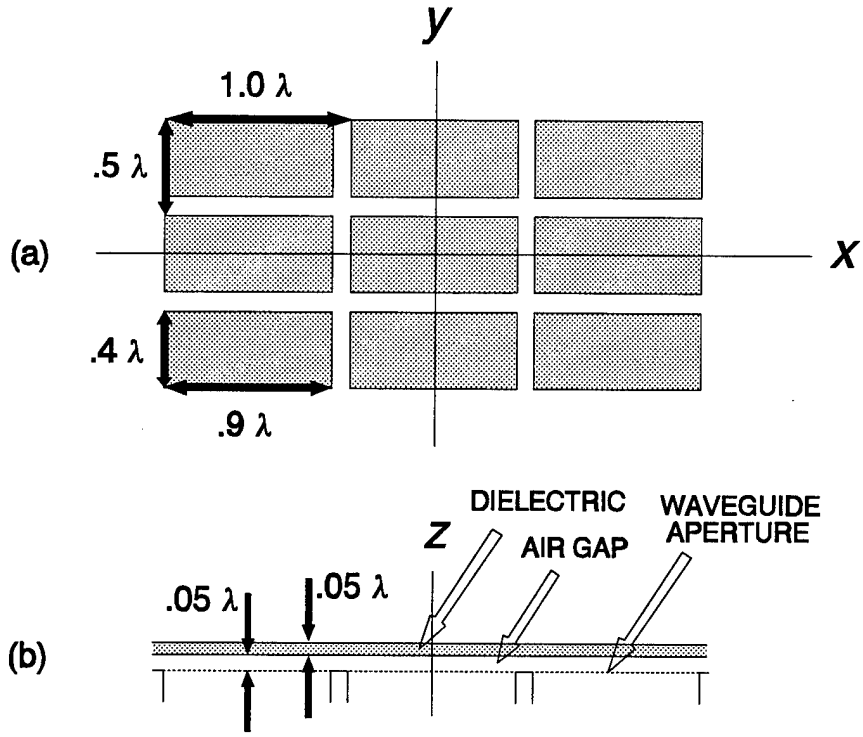

Figure 8. Geometry of Rectangular Waveguide Array with Air Gap and Dielectric Layer: (a) Top View; (b) Side View

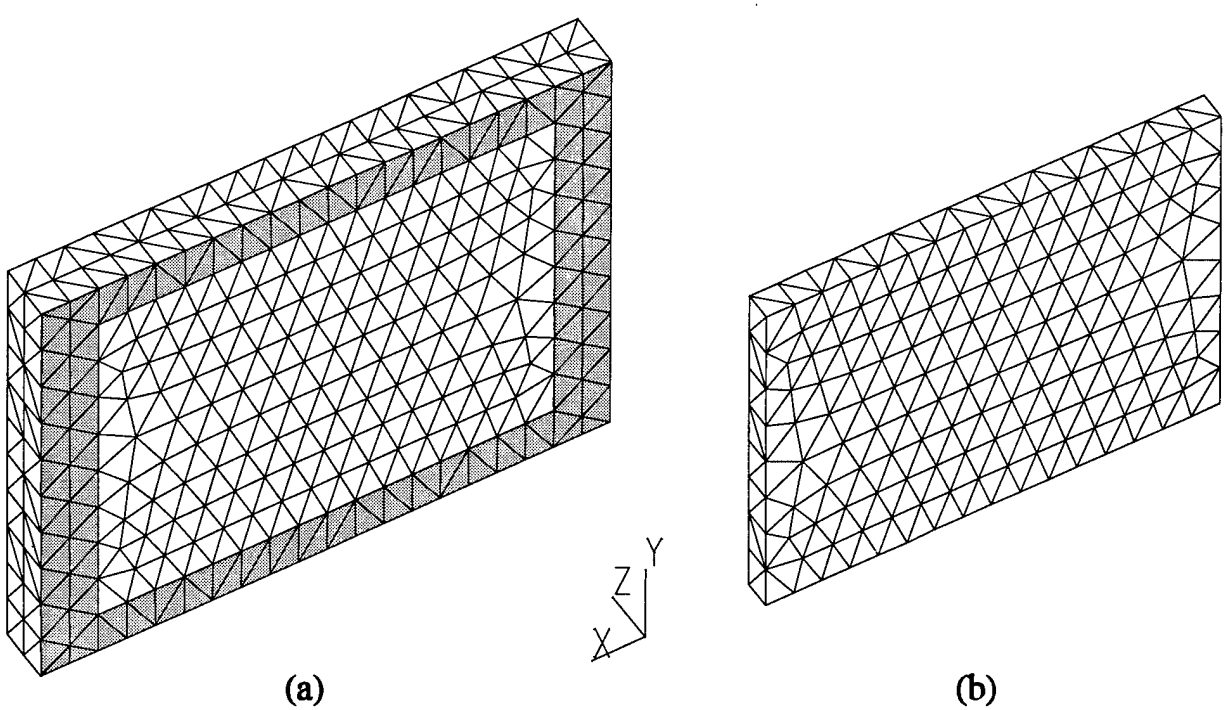

Figure 9. Mesh Models for Rectangular Waveguide Array: (a) Unit Cell Section Above Aperture; (b) Waveguide Section Below Aperture

dielectric layer. The shaded area is the ground plane's conducting surface outside the radiating aperture. Periodicity conditions are imposed on the unit cell side walls parallel to z. That is the approach that was previously necessary. In contrast, Fig. 9b shows the new alternative, in which the mesh is a single layer of cells inside the waveguide.

Figure 10 is a comparison of the calculated results for active reflection coefficient magnitude using both models, with the "radome" layer having permittivity of 1.0 and 4.0. In each case, the incident field is the TE_{10} mode, whose electric field is oriented in the y direction. The fact that these calculations agree confirms the validity of the recursion formula (30) for effective admittance used in the matrix fill computations.

Figure 11 compares the magnitude of the active element gain versus scan angle for the two cases. The agreement between these results establishes the validity of (70), the transmission coefficient for multiple layers. The phases of both the reflection and

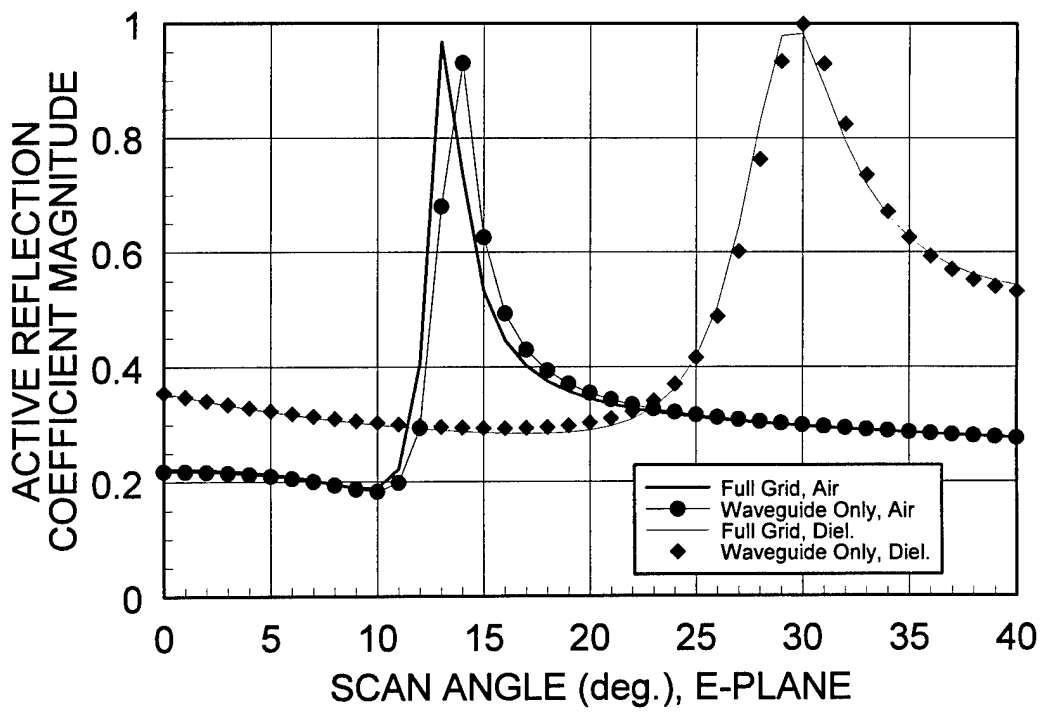

Figure 10. Active Reflection Coefficient Magnitude Calculated Using Alternative Models from Figure 9

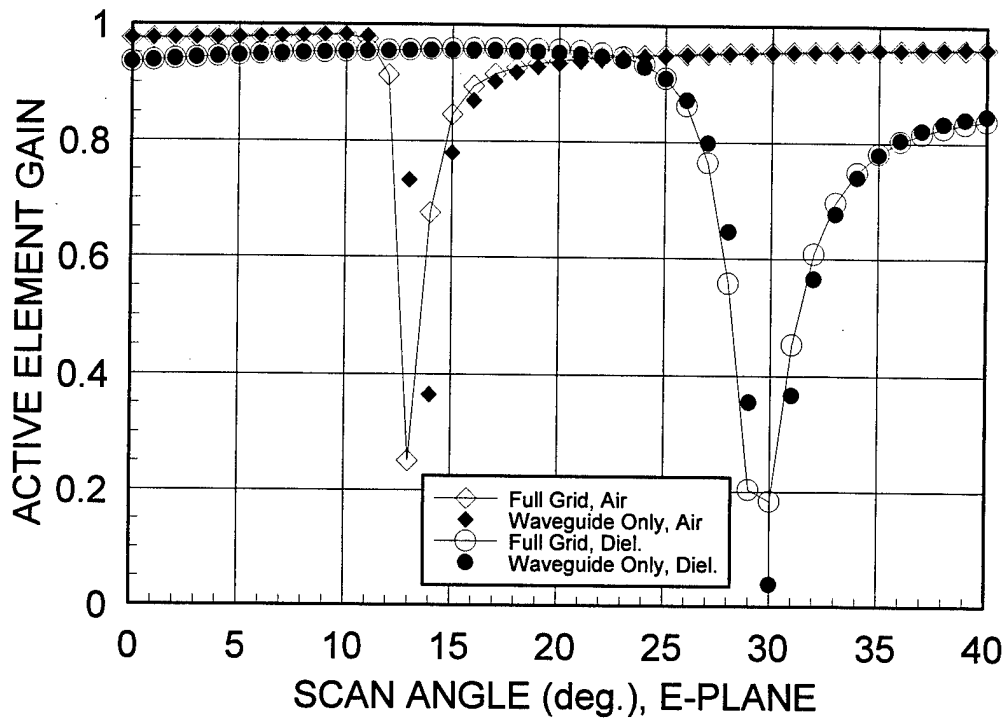

Figure 11. Active Element Gain Calculated Using Alternative Models from Figure 9

transmission coefficients exhibit similar behavior, although with offsets appropriate to the difference in reference locations. The incident field is referenced to Γ_A, which is different in the two cases. The transmitted field phase reference is at Γ_B (.1 λ above the ground plane) for the grid in Fig. 9a. For the grid in Fig. 9b, the transmission phase is referenced to the outer surface of the dielectric when one is present; or to the ground plane when it is absent.

The table below compares the two models' sizes and execution times. The new method results in a factor of 5 time savings for this problem. Furthermore, the mesh density was the same in each case, appropriate to the required density in the dielectric layer. That density is excessive for the waveguide model, which contains free space cells only. In situations involving thin, dense dielectrics, the results would even more dramatically favor the new approach.

Table I. Comparison of Size and Execution Time for Two Models of Rectangular Waveguide Array Antenna with Offset Dielectric Layer

Model	Mesh Edges (N)	Edges in Port A	Edges in Port B	Average Iterations	Average CPU secs.
Unit Cell (9a)	3841	381	690	.112 N	354
Waveguide (9b)	1449	381	381	.116 N	70

3.2.2. Reflection

To validate the formulas for the incident field arriving through an exterior dielectric layer, the array reflection case is examined. The receive case is modeled, in which the incident field is a plane wave impinging on the array face from the -z half space. By reversing the orientation of the model in Figure 9a, it may be used to simulate reflection from the same waveguide array antenna. The model in Figure 9b remains the same, with the boundary conditions on each side reversed. The former case is the reference solution since it uses the pre-existing, validated methods.

Figure 12 compares the active element gain (power coupled into the waveguide) using the two different mesh models, for scanning (direction of incidence) in both the E (y-z) and H (x-z) planes. As expected, the E plane results are identical to those in Figure 11. The correspondence between the two models indicates that the recursive formula for the incident field (58) is correct.

This concludes the discussion of computer code validation. The three cases presented above, circular waveguide array radiation, rectangular waveguide array radiation, and rectangular waveguide array reflection, verify the three essential developments that were needed to extend the existing theory to handle all configurations of stratified exterior dielectrics.

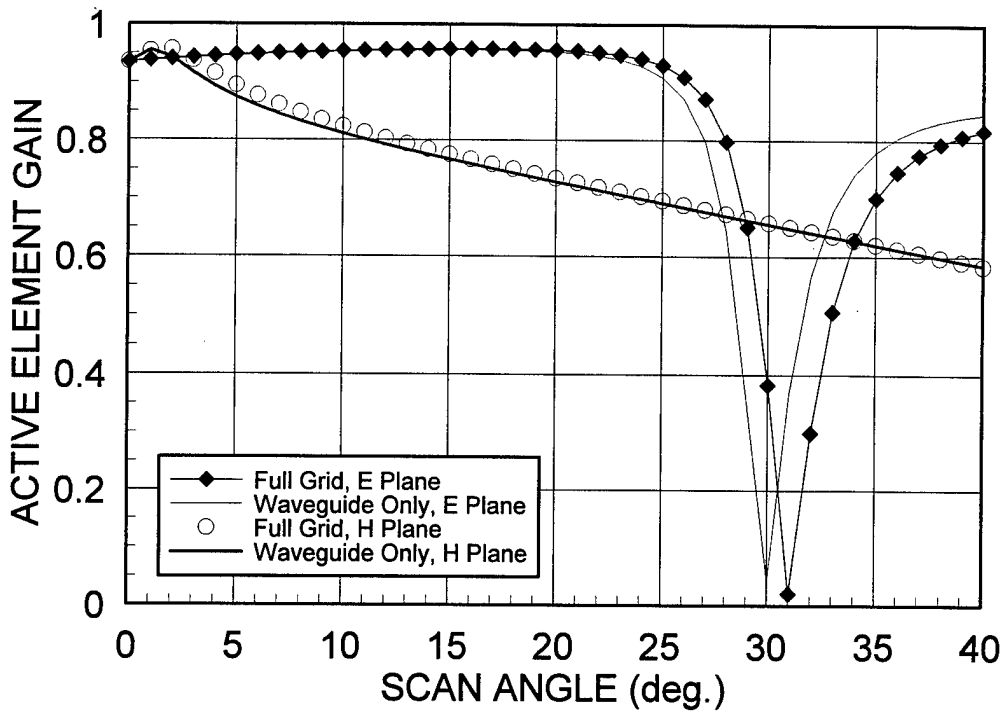

Figure 12. Received Power (Active Element Gain) Calculated Using Alternative Models from Figure 9 for Plane Wave Incidence

4. CONCLUSIONS

A method for incorporating the effects of exterior stratified dielectric layers in hybrid finite element calculations for periodic structures has been developed and demonstrated. This extension to the method makes it more efficient for modeling antennas that have wide-angle matching layers and/or radomes. It was previously necessary to extend the finite element mesh through all such layers, adding to the problem size and execution time.

Three modifications to the existing theory were required. First, the modal admittances used in computing the matrix terms for a periodic radiation boundary were replaced with effective admittances that account for the discontinuities between dielectric layers, and the layer thicknesses. Second, a similar effective admittance was derived for the incident field, which affects the calculation of the right-hand-side vector in the matrix equation. Last, after the matrix solution yields the coefficients for the electric field, the transmission and reflection coefficients are computed using a modified formula that includes multiplication of admittance ratios for each layer.

The foregoing extensions to the theory were demonstrated to be valid using an updated version of an existing hybrid finite element computer code. Calculations of active reflection coefficient and active element gain for both transmitting and receiving waveguide antenna arrays were shown to be correct. These calculations also demonstrated a factor of five savings in execution time for an array antenna with a radome.

APPENDIX A

NUMERICALLY STABLE ADMITTANCE COMPUTATION

Calculation of the effective admittance for external dielectric layers involves terms of the form:

$$\frac{Y^{/}}{Y^{M}} = \frac{\cos(z) + jA\sin(z)}{A\cos(z) + j\sin(z)} \tag{71}$$

where $z = x + jy$ and $A = Y^M/Y^A$. When z is large (in magnitude) and complex, which will be true for large orders of mode indices m and n, the complex cosine and sine functions may cause floating point overflow because they involve hyperbolic functions. To avoid that difficulty, the identities:

$$\cos z = \cos x \cosh y - j\sin x \sinh y \tag{72}$$

$$\sin z = \sin x \cosh y - j\cos x \sinh y \tag{73}$$

are used to rewrite (18) as

$$\frac{Y^{/}}{Y^{M}} = \frac{\cos(x)\left[1 - A\tanh(y)\right] + j\sin(x)\left[A - \tanh(y)\right]}{\cos(x)\left[A - \tanh(y)\right] - j\sin(x)\left[1 - A\tanh(y)\right]} \tag{74}$$

In computing the hyperbolic tangent, one of the following two forms is used:

$$\tanh(y) = \frac{e^{y} - e^{-y}}{e^{y} + e^{-y}} = \frac{1 - e^{-2y}}{1 + e^{-2y}} \tag{75}$$

$$= \frac{e^{2y} - 1}{e^{2y} + 1} \tag{76}$$

choosing (22) for $y \geq 0$ or (23) for $y \leq 0$.

REFERENCES

1. McGrath, Daniel T., "Electromagnetic Analysis of Periodic Structure Reflection and Transmission by the Hybrid Finite Element Method," USAF Phillips Laboratory, Kirtland AFB, NM, Sept. 1995, PL-TR-95-1103. Summarized in: D.T. McGrath and V.P. Pyati, "Periodic Structure Analysis Using a Hybrid Finite Element Method," *Radio Science*, **31**, pp. 1173-1179, Sep-Oct 1996.

2. Amitay, Noach, Victor Galindo and Chen-Pang Wu, *Theory and Analysis of Phased Array Antennas*, Wiley Interscience, 1972.

3. Mittra, Raj, Chi H. Chan, and Tom Cwik, "Techniques for Analyzing Frequency Selective Surfaces--A Review," *Proceedings of the IEEE*, **76**, pp. 1593-1615, Dec. 1988.

4. Marcuvitz, Nathan, *Waveguide Handbook*, New York: McGraw-Hill, 1951 and London: Peregrinus, 1986.

5. McGrath, Daniel T., "Hybrid Finite Element/Waveguide Mode Analysis of Passive RF Devices," USAF Rome Laboratory, Griffiss AFB, NY, Jul. 1993, RL-TR-93-130.

6. McGrath, Daniel T., "Phased Array Antenna Analysis Using Hybrid Finite Element Methods," PhD Dissertation, AF Institute of Technology, Wright-Patterson AFB, OH, Ju. 1993, AFIT/DS/ENG93-4. Summarized in: D.T. McGrath and V.P. Pyati, "Phased Array Antenna Analysis with the Hybrid Finite Element Method," *IEEE Transactions on Antennas and Propagation*, **AP-42**, pp. 1625-1630, Dec. 1994.

7. Sarkar, Tapan K., "On the Application of the Generalized BiConjugate Gradient Method," *Journal of Electromagnetic Waves and Applications*, Vol. 1, pp. 223-242, 1987.

DISTRIBUTION LIST

Addressee	Copies
Capt Peter Collins AFIT/ENG wright-Patterson AFB, OH 45433-7765	1
Dr Vittal Pyati AFIT/ENG Wright-Patterson AFB, OH 45433-7765	1
Dr William Baker AFIT/ENM Wright-Patterson AFB, OH 45433-7765	1
Dr Arje Nachman AFOSR/NM Bolling AFB, DC 20332	1
Dr Clifford Rhoades AFOSR/NM Bolling AFB, DC 20332	1
AFSAA/SAI Washington, DC 20330-1580	1
Mr Ronald Chase AMSRL-SE-DE Adelphi, MD 20783-1197	1
AUL/LSE Maxwell AFB, AL 36112-6424	1
Mr Tom Blalock DIA/MSIC Redstone Arsenal, AL 35898-5500	1
DTIC/OCP Ft. Belvoir, VA 22060-6218	2
Dr Helen Wang Naval Air Warfare Center China Lake, CA 93555-6001	1
Dr. C. Long Yu Naval Air Warfare Center Point Mugu, CA 93042-5000	1
Dr Richard Adler Naval Postgraduate School Monterey, CA 93943	1
Dr David Jenn Naval Postgraduate School Monterey, CA 93943	1
Dr Eric Mokole Naval Research Laboratory 4555 Overlook Ave SE Washington, DC 20375	1

Addressee	Copies
Dr William Pala Naval Research Laboratory 4555 Overlook Ave SE Washington, DC 20375	1
Dr Charles Manry NCCOSC RDT&E Div 53225 Millimeter St, Rm 32 San Diego, CA 92152-7313	1
Dr Jay Rockway NCCOSC RDT&E Div 53225 Millimeter St, Rm 32 San Diego, CA 92152-7313	1
Dr Michael Schuh NASA Ames Research Center Moffett Field, CA 94035-1000	1
Dr Alex Woo NASA Ames Research Center Moffett Field, CA 94035-1000	1
AFRL/PSOTH Kirtland AFB, NM 87117-5776	1
AFRL/PSOTL Kirtland AFB, NM 87117-5776	2
Dr William Baker AFRL/DEH Kirtland AFB, NM 87117-5776	1
Dr Patrick McDaniel AFRL/DEPA Kirtland AFB, NM 87117-5776	1
Mr Jeff MacGillivray AFRL/DEPE Kirtland AFB, NM 87117-5776	1
Mr Joseph Sadler AFRL/DEPE Kirtland AFB, NM 87117-5776	1
Mr Kerry Sandstrom AFRL/DEPE Kirtland AFB, NM 87117-5776	1
Dr Moossa Arman AFRL/DEHE Kirtland AFB, NM 87117-5776	1
Dr Leon Chandler AFRL/DEHE Kirtland AFB, NM 87117-5776	1

Capt Karyl Davis
AFRL/DEHA 1
Kirtland AFB, NM 87117-5776

Lt Aimee Gibbs
AFRL/DEHE 1
Kirtland AFB, NM 87117-5776

Dr Michael Haworth
AFRL/DEHE 1
Kirtland AFB, NM 87117-5776

Dr Kyle Hendricks
AFRL/DEHE 1
Kirtland AFB, NM 87117-5776

Dr Thomas Hussey
AFRL/DEHA 1
Kirtland AFB, NM 87117-5776

Dr Diana Loree
AFRL/DEHE 1
Kirtland AFB, NM 87117-5776

Official Record Copy
AFRL/DEHE 10
Kirtland AFB, NM 87117-5776

Dr Thomas Spencer
AFRL/DEHE 1
Kirtland AFB, NM 87117-5776

Capt Gerald Sasser
AFRL/DEHE 1
Kirtland AFB, NM 87117-5776

Capt Laurence Merkle
AFRL/DEHE 1
Kirtland AFB, NM 87117-5776

Dr Robert Peterkin
AFRL/DEHE 1
Kirtland AFB, NM 87117-5776

Ms Michelle Champion
AFRL/SNHA 1
Hanscom AFB, MA 01731-3010

Dr Jeffrey Herd
AFRL/SNHA 1
Hanscom AFB, MA 01731-3010

Dr Hugh Southall
AFRL/SNHA 1
Hanscom AFB, MA 01731-3010

Dr Hans Steyskal
AFRL/SNHA 1
Hanscom AFB, MA 01731-3010

Dr Peter Franchi
AFRL/SNHA 1
Hanscom AFB, MA 01731-3010

Dr Robert Mailloux
AFRL/SNH 1
Hanscom AFB, MA 01731-3010

Dr Boris Tomasic
AFRL/SNHA 1
Hanscom AFB, MA 01731-3010

Dr Donald Pflug
AFRL/IFSB 1
Rome, NY 13441-4505

Dr Chris Reuter
AFRL/IFSB 1
Rome , NY 13441-4505

Dr Dale Coleman
Sandia Nat'l Lab 1
Albuquerque, NM 87185

Dr Ray Lemke
Sandia Nat'l Labs 1
Albuquerque, NM 87185

Capt Michael Walker
USAFA/DFEE 1
USAF Academy, CO 80840-6236

Mr Jeff Hughes
AFRL/SN 1
2010 5th St
Wright-Patterson AFB, OH 45433-6523

Dr Joseph Shang
AFRL/VA 1
2645 5th St, Ste 7
Wright-Patterson AFB, OH 45433-7913

Dr Kwang Min
AFRL 1
Eglin AFB, FL 32542-5434

Dr Kueichien Hill
AFRL/XPN 1
2591 K St
Wright-Patterson AFB, OH 45433-7602

Dr Brian Kent
AFRL/XPN 1
2591 K St
Wright-Patterson AFB, OH 45433-7602

Mr Ed Utt
AFRL/XPN 1
2591 K St
Wright-Patterson AFB, OH 45433-7602

Mr Min Lee
Joint STARS Project Mgr 1
Ft. Monmouth, NJ 07703-5304

Dr David Auckland
Atlantic Aerospace Electronics 1
Greenbelt, MD 20770-1406

Dr Janice Karty
Boeing 1
PO Box 516
St. Louis, MO 63166

Dr Shung-Wu Lee
DEMACO 1
100 Trade Center
Champaign, IL 61820

Mr Kevin Long
Dynetics 1
Huntsville, AL 35184

Dr J.P. Montgomery
EMS Technologies 1
PO Box 7700
Norcross, GA 30091-7700

Mr Tim Durham
Harris GASD 1
PO Box 94000
Melbourne, FL 32902

Mr Steve Panaretos
Huques Aircraft Co MS RE/R2/V518 1
PO Box 92426
Los Angeles, CA 90009

Dr Tom Cwik
Jet Propulsion Laboratory 1
4800 Oak Grove Dr
Pasadena, CA 91109-8099

Dr Cinzia Zuffada
Jet Propulsion Laboratory 1
4800 Oak Grove Dr
Pasadena, CA 91109-8099

Mr Robert Rupp
Lockheed-Martin 1
199 Borton Landing Rd
Moorestown, NJ 08057-0927

Dr Vaughn Cable
Lockheed-Martin 1
1011 Lockheed Way
Palmdale, CA 93599-2550

Dr Don Spencer
Lockheed-Martin Sanders 1
PO Box 868
Nashua, NH 03061-0868

Dr Leo Kempel
Mission Research Corp. 1
147 John Sims Parkway
Valparaiso, FL 32580

Dr. Glen Salo
Mission Research Corp. 1
3975 Research Blvd
Dayton, OH 45430

Mr D Hohanshelt
Motorola Gov't Systems 1
8201 E McDowell Rd
Scottsdale, AZ 85257

Dr Maurice Sancer
Northrop-Grumman 1
8900 E Washington Blvd
Pico Rivera, CA 90660-3737

Mr Fernando Beltran
Raytheon 1
528 Boston Post Rd
Sudbury, MA 01776

Dr Oren Kesler
Raytheon TI Systems 1
2501 W University
McKinney, TX 75070

Dr Hormoz Mohammadian
Rockwell Science Center 1
Thousand Oaks, CA 91358

Mr Henry Grass
Teledyne Brown Engineering 1
300 Sparkman Dr
Huntsville, AL 35807

Prof Jianming Jin
University of Illinois 1
1406 W Green St
Urbana, IL 61801-2991

Prof John Volakis
University of Michigan 1
1301 Beal Ave
Ann Arbor, MI 48109-2122